Acta Materialia 134 (2017) 31–39

Contents lists available at ScienceDirect

Acta Materialia

journal homepage: www.elsevier.com/locate/actamat

# Using complimentary microscopy methods to examine Ni-Mn-Si-precipitates in highly-irradiated reactor pressure vessel steels☆

P.D. Edmondson*, C.M. Parish, R.K. Nanstad

*Materials Science & Technology Division, Oak Ridge National Laboratory, Oak Ridge, TN 37831, USA*

ARTICLE INFO

*Article history:*
Received 22 February 2017
Received in revised form
27 April 2017
Accepted 22 May 2017
Available online 29 May 2017

*Keywords:*
Precipitation
Atom probe tomography
Scanning/transmission electron microscopy
Multivariate statistical analysis
RPV steels

ABSTRACT

Nano-scale Ni-Mn-Si-rich precipitates formed in a reactor pressure vessel steel under high neutron fluence have been characterized using highly complimentary atom probe tomography (APT) and scanning transmission electron microscopy with energy dispersive spectroscopy (STEM-EDS) combined with STEM-EDS modeling. Using these techniques in a synergistic manner to overcome the well-known trajectory aberrations in APT data, the average upper limit Fe concentration within the precipitates was found to be ~6 at.%. Using this knowledge, accurate compositions of the precipitates was determined and it was found that the spread of precipitate compositions was large, but mostly centered around the $\Gamma_2$-and *G*-phases. The use of STEM-EDS also allowed for larger areas to be examined, and segregation of minor solutes was observed to occur on grain boundaries, along with Ni-Mn-Si-rich precipitates that were smaller in size than those in the matrix. Solute segregation at the grain boundaries is proposed to occur through a radiation induced segregation or radiation enhanced diffusion mechanism due to the presence of a denuded zone about the grain boundary. It is also proposed that the reduced precipitate size at the grain boundaries is due to the structure of the grain boundary. The lack of Ni-Mn-Si precipitates observed in larger Mo-rich precipitates is also discussed, and the absence of the minor solutes required to form the Ni-Mn-Si precipitates results in the lack of nucleation. This is in contrast to cementite phases in which Ni-Mn-Si precipitates have been observed to have formed. It was also determined through this work that the exclusion of all the Fe ions during atom probe analysis is a reasonable approximation.

Published by Elsevier Ltd on behalf of Acta Materialia Inc.

## 1. Introduction

The reactor pressure vessel (RPV) of light-water-type nuclear reactors (LWR) are critical components, and contribute to the containment solution of off-normal operations, in which case they must not fail [1]. However, these RPV's are subjected to significant neutron irradiation at elevated temperatures (~300 °C) over the course of their lifetime. This combination of elevated temperature, and neutron-induced displacement of the atomic lattice can lead to the formation of defects and other microstructural features – primarily clustering and precipitation of the minor solutes – that can be significantly detrimental to the mechanical properties of the RPV, e.g. embrittlement, that may lead to failure. It is, therefore, necessary to develop a detailed understanding of the nature of the formation and nature of these defects/microstructures in order to design new materials and/or mitigation strategies to enable lifetime extensions for nuclear power plants, particularly as the cost to replace and dispose of a RPV would be prohibitively expensive.

In low-alloy steels, such as those used for both the forging and welds in RPVs, small concentrations of Ni, Mn, Si, and Cu are typically present [2]. However, under irradiation, these solutes undergo radiation-induced clustering forming Cu-rich precipitates (commonly referred to as CRPs) and Ni-Mn-Si-rich precipitates (NMS). These NMS precipitates are thought to nucleate based on a heterogeneous nucleation model in which the precipitates nucleate within the damage cascades induced by neutron irradiation, as defect-cluster complexes or their defect-free remnants [3–5].



* Corresponding author.
*E-mail address:* edmondsonpd@ornl.gov (P.D. Edmondson).

http://dx.doi.org/10.1016/j.actamat.2017.05.043
1359-6454/Published by Elsevier Ltd on behalf of Acta Materialia Inc.

NMS precipitates have been observed in a wide range of RPV steel compositions, including Western [6–8], Russian [9–11] and model compositions [12] under elevated temperature neutron irradiation. Recently, it has been observed that NMS precipitates formed in the cementite phase of model RPV steels that had undergone long term thermal aging [2]. These thermally formed NMS precipitates were only observed to form in cementite phase and not the ferrite, and had compositions that were different to those observed in irradiated RPV steels. CRPs are observed only to form in materials with concentrations of copper, typically above 0.05 at.% [6].

Detailed, high-fidelity characterization of both CRP's and NMS precipitates in RPV steels is critical to the understanding of their formation and dissolution in order to preserve structural integrity of the RPVs. Typically atom probe tomography (APT) and small-angle neutron scattering (SANS) have been extensively applied for characterization of the fine-scale precipitates. These techniques are subject to key uncertainties and user inputs that may either influence the results, or lead to the development of different conclusions, as discussed by Hyde et al. [13] However, both techniques provide invaluable information when used correctly: APT provides three dimensional atom-by-atom reconstructions along with chemical information allowing precipitation and segregation to be clearly observed, yet only in relatively small volumes; SANS allows for a much broader view, but without the fine scale detail information. Hence these two techniques can be complimentary.

Another analytical method for characterizing CRP's and NMS precipitates is the use of scanning/transmission electron microscopy with energy dispersive X-ray spectroscopy (STEM-EDS), combined with advanced data mining techniques such as multivariate statistical analysis (MVSA). A low alloy A508 Gr4N forging steel irradiated to very low fluence was previously characterized using STEM-EDS combined with MVSA [14], however the instrumentation at the time limited the quality of the data collected (spectrum images were collected over a 128×128 pixel area, using an EDS detector with a solid angle of 0.3 srad).

Here, a detailed analysis of a high nickel, low copper RPV weld surveillance specimen, irradiated to high fluence in a commercial power reactor, is characterized using the complementary techniques of APT, and STEM-EDS combined with MVSA and X-ray simulation to provide a deeper insight into the local chemistry of the NMS precipitates, specifically focusing on the Fe content within the precipitates thereby facilitating more detailed modeling to support the prediction of the formation of the precipitates, and their direct effects on mechanical property changes of the RPV steels.

## 2. Experimental methods

### 2.1. Material & irradiation

The material examined was part of the surveillance campaign for the Ringhals Nuclear Power Plant Unit 3 reactor, and is a high-Ni, low-Cu weld specimen having the composition given in Table 1. The material was irradiated during normal power generating operations at a temperature of 284 °C to a total fluence of $6.39 \times 10^{23}$ n m$^{-2}$ (E > 1 MeV) equivalent to 13.8 effective full power years, EFPY, at a flux of $1.47 \times 10^{15}$ n m$^{-2}$ s$^{-1}$ [7,15]. This material is of particular interest due to the observed significant radiation sensitivity, as indicated by the very high Charpy 41-J transition temperature shift, $\Delta T_{41-J}$, of 192 °C at $5.0 \times 10^{23}$ n m$^{-2}$ [15].

### 2.2. Atom probe tomography

Atom probe tomography (APT) was conducted on needle-shaped specimens prepared using standard electropolishing techniques [16] with the use of small blanks cut from the bulk material. The electrolyte used for the polishing was a solution of 2% perchloric acid in 2-butoxyethanol, and polishing was conducted at room temperature at 15 VDC.

Atom probe characterization was conducted using a Cameca Instruments LEAP 4000X HR. All data were recorded in voltage pulsing mode, using a specimen temperature of 50 K, a pulse repetition rate of 200 kHz, an ion collection rate of between 0.5 and 1 ions per pulse, and a pulse fraction of 0.2 [7]. Reconstructions of the data was performed using Cameca's IVAS version 3.6.8 based on a standard reverse-point-projection algorithm. To search for the nano-scale Ni-Mn-Si precipitates, the maximum separation method [17] was used with the search parameters determined using the methodology of Bachhav et al. [18] This involved identifying search parameters for each individual dataset based on the first-order nearest neighbor distribution (For the dataset shown in Fig. 1b, a $d_{max}$ of 0.58 nm, and $N_{min}$ of 20 were used in the maximum separation cluster search analysis). Further analysis was conducted using a custom MATLAB script with radii, number densities, and volume fractions being calculated from the maximum separation output file based on the ranged ion count within the precipitates, and assuming the precipitates have the same atomic density as the ferrite matrix (84.3 atoms nm$^{-3}$). Compositions, such as that given in Table 1, were determined using appropriate ranging of the mass

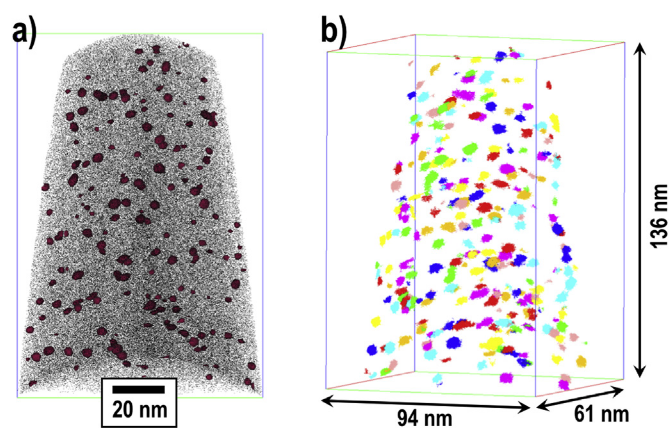


**Fig. 1.** Atom probe reconstructions of the analysis volume: a) atom map showing 1.2% Fe atoms represented as black dots, and a 13% concentration isosurface highlighting the positions and relative sizes of the Ni-Mn-Si-rich precipitates; and b) indexed clusters from the same dataset, as determined using the maximum separation method.

**Table 1**
Composition of the Ringhals Unit 3 reactor weld metal from the surveillance program used in this study as determined from the atom probe tomography results. The balance is Fe.

| | Ni | Mn | Si | Cu | P | C | Cr | Mo | S | V | Co |
|---|---|---|---|---|---|---|---|---|---|---|---|
| wt.% | 1.580 | 1.227 | 0.204 | 0.057 | 0.007 | 0.004 | 0.239 | 0.191 | 0.111 | 0.002 | 0.017 |
| at.% | 1.501 | 1.245 | 0.405 | 0.050 | 0.013 | 0.018 | 0.256 | 0.111 | 0.193 | 0.002 | 0.016 |